Available online at www.sciencedirect.com
ScienceDirect
International Journal of Heat and Mass Transfer 50 (2007) 1–14
International Journal of HEAT and MASS TRANSFER
www.elsevier.com/locate/ijhmt

Two-phase flow in converging and diverging microchannels with CO_2 bubbles produced by chemical reactions

B.R. Fu, F.G. Tseng, Chin Pan *

Department of Engineering and System Science, National Tsing Hua University, Hsinchu 30043, Taiwan, ROC

Received 24 March 2006; received in revised form 30 June 2006
Available online 25 September 2006

Abstract

The present study investigates experimentally the evolution of two-phase flow pattern and pressure drop in the converging and diverging, silicon-based microchannels with mean hydraulic diameter of 128 μm and CO_2 bubbles produced by chemical reactions of sulfuric acid (H_2SO_4) and sodium bicarbonate ($NaHCO_3$). Three different concentrations of 0.2, 0.5 and 0.8 mol/L of each reactant at the inlet before mixing and 10 different flow rates from 1.60×10^{-9} m^3/s to 16.0×10^{-9} m^3/s are studied. Flow visualization is made possible by using a high-speed digital camera. It is found that the present design of the microchannel, with the inlet chamber, results in much more intensive chemical reactions in the diverging microchannel than that in the converging one. The void fractions at the entrance and exit regions and pressure drop through the channel are also measured. The results reveals that the presence of small void fraction, <0.1, at the inlet may promote CO_2 generation in the microchannel, irrespective of the channel is converging or diverging, indicating the agitation effects of bubbly flow in the microchannel. The increase of inlet concentration of reactants does not increase the pressure drop in the converging microchannel significantly, while the inlet concentration presents significant but mild effects on the pressure drop in the diverging microchannel. The two-phase frictional multiplier may be positively correlated with the mean void fraction in the channel linearly, and the data agree well with predictions from the correlations in the literature.

Keywords: Microchannel; Two-phase flow; Two-phase frictional multiplier

1. Introduction

Direct methanol fuel cells (DMFCs) have shown good potential serving as power supplies for computer, communication and consumer electronics (3C) products due to their high energy density. The oxidation of methanol in the anode area will, however, inevitably generate carbon dioxide and the removal of CO_2 bubbles is of critical concern for the development of a micro DMFC. The CO_2 bubbles may result in the blockage of the anode structure and significantly influence the performance of a micro DMFC [1].

Recently, there have been very active research activities on gas–liquid two-phase flow in minichannels or microchannels. For example, Fukano and Kariyasaki [2], and Mishima and Hibiki [3] studied air/water two-phase flow pressure drop in minichannels. Triplett et al. [4,5] investigated air/water two-phase flow patterns, void fraction and two-phase flow pressure drop in minichannels. Chen et al. [6] investigated experimentally nitrogen/water two-phase flow pattern, bubble speed and void fraction in a glass capillary (minichannel). Using a high speed video camera, they were able to measure the bubble speed accurately. With both the bubble speed and superficial gas velocity measured, the void fraction can be determined accurately according to its basic definition. Stanley et al. [7] studied two-phase flow of water and gas (argon, helium or nitrogen) in rectangular microchannels. Serizawa et al. [8] explored air/water two-phase flow in circular tubes of 20, 25 and 100 μm. Several distinctive flow patterns were reported and the flow pattern was found to be sensitive

* Corresponding author.
E-mail address: cpan@ess.nthu.edu.tw (C. Pan).

0017-9310/$ - see front matter © 2006 Elsevier Ltd. All rights reserved.
doi:10.1016/j.ijheatmasstransfer.2006.06.029

Nomenclature

C	mole concentration of reactant at the inlet before mixing (mol/L)
C_f	a fitting constant
D_H	hydraulic diameter of the microchannel (m)
f	friction factor
L	length of the microchannel (m)
M	Chisholm's parameter
Q_H	volume flow rate of sulfuric acid (m^3/s)
Q_N	volume flow rate of sodium bicarbonate (m^3/s)
Re	Reynolds number
V	velocity of fluid (m/s)
V_{in}	velocity of fluid in the inlet (m/s)
V_{out}	velocity of fluid in the outlet (m/s)
X	Lockhart–Martinelli parameter
x	quality in the channel
x_{ave}	average quality
x_{in}	quality in the inlet region
x_{out}	quality in the outlet region

Greek symbols

α_{in}	void fraction in the inlet region
α_{out}	void fraction in the outlet region
ΔP_f	frictional pressure drop (Pa)
$\Delta P_{f,2\phi}$	two-phase frictional pressure drop (Pa)
$\Delta P_{f,L}$	single phase frictional pressure drop (Pa)
ΔP_{in}	pressure loss at the inlet (Pa)
ΔP_{total}	total pressure drop (Pa)
ΔP_{out}	pressure loss at the outlet (Pa)
ϕ_L^2	two-phase frictional multiplier
γ	aspect ratio of the depth to the width of the channel
μ_L	viscosity of liquid mixture (Pa s)
ρ	density of fluid (kg/m^3)
ρ_G	density of CO_2 (kg/m^3)
ρ_L	density of liquid mixture (kg/m^3)

to the surface conditions. Chung and Kawaji [9] investigated the effect of channel diameter on water/nitrogen two-phase flow in circular microchannels of 530, 250, 100 and 50 μm diameters. Fu and Pan [10] explored experimentally the two-phase flow with CO_2 bubbles generated by the chemical reactions of sulfuric acid and sodium bicarbonate in a rectangular microchannel with uniform cross section. The flow pattern transition instability between bubbly-slug and slug flow was reported for the cases with highest inlet concentration, i.e., $C = 0.8$ mol/L, and low flow rates.

Due to acceleration or deceleration effects, transport of bubbles in a converging or diverging microchannel may be significantly different from that in a microchannel with uniform cross section. Lin et al. [11] reported the bubble movement in a short diverging microchannel. They attributed the movement of the bubble to a large cross section to the interfacial tension force. Hwang et al. [12] explored the two-phase flow characteristics of ethanol/CO_2 in a converging or diverging microchannel with mean hydraulic diameters of 122 and 105 μm, respectively. Two-phase flow patterns and pressure drop in converging and diverging microchannels were investigated. They found that the acceleration effect and so the steep pressure gradient in a converging microchannel may result in the elongation of bubbles in slug flow, while the deceleration effect and so the possible pressure rise in the diverging microchannel causes shortening of bubbles in slug flow significantly. For both types of microchannel, the collision and merger of two consecutive bubbles may take place and result in twisting of bubbles.

Following the work of Hwang et al. [12], the present study investigates experimentally the two-phase flow characteristics in a converging or diverging microchannel with CO_2 bubbles generated by chemical reactions of sulfuric acid and sodium bicarbonate:

$$H_2SO_4 + 2NaHCO_3 \rightarrow Na_2SO_4 + 2H_2O + 2CO_2 \quad (1)$$

Such a bubble formation from chemical reactions may simulate more closely the transport phenomena of CO_2 bubble in a micro DMFC than that of Hwang et al. [12]. Meng et al. [13] employed the same chemical reaction to produce CO_2 bubbles in a stagnant system to study the removal of CO_2 bubbles.

The chemical reaction will take place in the microchannel while the reactant solutions flow through it and results in generation of CO_2 in the microchannel. Such a kind of CO_2 generation while flowing with acceleration or deceleration effects, which have been shown to have significant influence on the two-phase flow characteristics [12], in the converging or diverging microchannel may result in interesting two-phase flow phenomena. Such two-phase flow phenomena with volumetric generation of CO_2 bubble formation may have significant implication for the CO_2 bubble transport in a micro DMFC. Moreover, the difference in chemical behavior between converging and diverging microchannels is of significant interest for the design micro reactor.

2. Experimental detail

2.1. Experimental setup

A schematic diagram of the experimental setup, consisting of the test section with a converging or diverging microchannel, syringe pump, flow visualization system and pressure measurement system, is shown in Fig. 1. The syringe pump with two syringe tubes drove the two solutions (H_2SO_4 and $NaHCO_3$), each at a flow rate given by the setting of the pump simultaneously to the inlet chamber at the

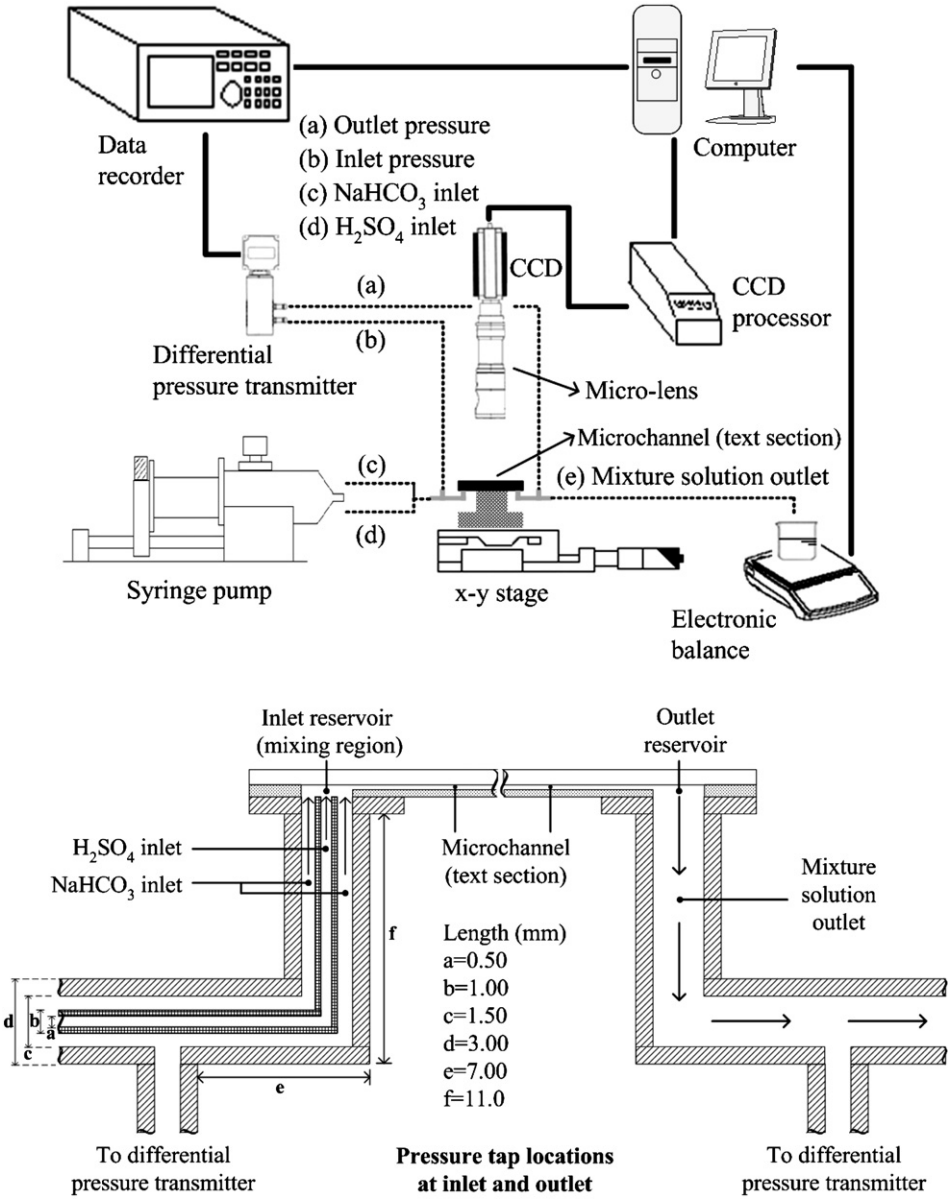

Fig. 1. Experimental apparatus and pressure measurement layout.

same flow rate through a concentric device, as shown in Fig. 1 with H_2SO_4 flowing in the central tube and $NaHCO_3$ in the annulus. The two fluids meet at the bottom of the inlet chamber and certain degrees of mixing may take place there. The exhausted fluids from the test section were drained to a container on an electronic balance, which might provide calibration of flow rate of each solution before an experiment. The pressure taps are located near the inlet or outlet at the connecting fixture as shown. The inside diameter of the connecting fixtures is much larger then the test channel, therefore, the pressure loss through them may be neglected. The differential pressure transducer (Huba 692) used in the present work is with a short response time of 0.005 s and the sampling rate for pressure drop measurement was set at 100 Hz. The geometric data of the test section are illustrated in Fig. 2(a) and 2(b) for

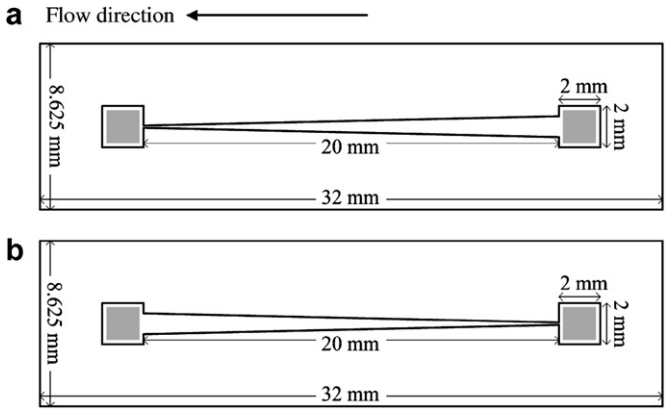

Fig. 2. Geometric data of the microchannel: (a) converging, (b) diverging microchannel (■: excimer laser-etched hole).

the converging and diverging microchannels, respectively. The converging microchannel width varied linearly from 1050 μm to 100 μm and from 100 μm to 1050 μm for the diverging one resulting a converging or diverging angle of 1.36°. The length and depth for both types of microchannel were 20 mm and 75 μm, respectively. The mean hydraulic diameter for both kinds of microchannel was the same of 128 μm.

The flow visualization system included a high-speed digital camera (KODAK motion coder SR-ultra), a monitor and a personal computer. A micro-lens was mounted on the CCD to observe the two-phase flow patterns in the diverging and converging microchannels. Moreover, an x–y–z mechanism was installed with the test module to hold the lens and provide accurate position on the test plane (x–y plane) and focusing (z-direction).

2.2. Fabrication of the test section

The test section was a 8.625 mm × 32 mm silicon stripe, which was made of P-type ⟨100⟩ orientation wafer. The fabrication process of the microchannel employed bulk micromachining and anodic bonding process. The microchannel and mixing regions, at the inlet and the exit, before and after the channel, were etched by using deep reactive ion etching. Subsequently, the direct writing of excimer laser micromachining technology was applied for the through hole under the mixing regions. To enable flow visualization, the top surface was covered with Pyrex #7740 glass through anodic bonding.

2.3. Experimental procedure

The present study employed aqueous solutions of sulfuric acid (H_2SO_4) and sodium bicarbonate ($NaHCO_3$) as the working fluids. Both reactant solutions were driven by syringe pump at the same flow rate. The volume flow rates for both solutions were controlled ranging from 1.60×10^{-9} m^3/s to 16.0×10^{-9} m^3/s. Three concentrations of both reactants at the inlet before mixing, C, of 0.2, 0.5 and 0.8 mol/L were investigated. The solution of sulfuric acid at a specific concentration was prepared by using 96% H_2SO_4 and solution of sodium bicarbonate using pure solid sodium bicarbonate in a powder form with appropriate amount of deionized water. For example, the concentration of 0.2 mol/L of the sodium bicarbonate solution was prepared by 0.2 mole of pure chemical compound dissolved in the de-ionized water to 1 liter. The employment of the same concentration for both reactants might consume thoroughly sodium bicarbonate in the channel and help the estimation the production rate of CO_2. The formula (1) suggests that 1 mole of sodium bicarbonate consumed could produced 1 mole of CO_2. If sodium bicarbonate were totally consumed, the volume flow rate of CO_2 produced would be 7.69×10^{-9} to 76.9×10^{-9} m^3/s, 19.2×10^{-9} to 192×10^{-9} m^3/s, 30.8×10^{-9} to 308×10^{-9} m^3/s, respectively, at the channel exit corresponding to $C = 0.2$, 0.5 and 0.8 mol/L depending on flow rate. These estimates were based on CO_2 being an ideal gas at 1 atm and 20 °C (room temperature). The evolution of two-phase flow patterns in both diverging and converging microchannels was visualized employing the high speed video camera. The typical frame rate used was 500 frames/s and the exposure time was 1/20,000 s. A 250 W fiber optic illuminator was used as the light source.

The projected area of bubbles on the bottom wall in each frame may be determined by edge detection manually of the boundary of bubbles and subsequently using Image Pro to obtain the area. The void fractions in the inlet and outlet regions of the channel were determined by the mean value of the projected area of bubbles of fifty frames randomly selected divided by the bottom surface area of the region. The void fraction was determined implicitly assumed that the bubble completely fill the volume of the projected area.

2.4. Measurement uncertainty

The measurement uncertainties for flow rate in the diverging and converging microchannels after calibration using a high precision electronic balance were estimated to be 0.33% and 0.21%, respectively. The measurement uncertainty of pressure transducer was 0.5%.

3. Results and discussion

3.1. Evolution of two-phase flow pattern

Channel profile, reactants concentration at the inlet, flow rate and inlet geometry have significant effects on the evolution of two-phase flow pattern along the microchannel. The volume flow rates for both solutions were controlled ranging from 1.60×10^{-9} m^3/s to 16.0×10^{-9} m^3/s. The residence time of both fluids in the microchannel is estimated to be from 0.027 to 0.270 s. As for the inlet chamber, the residence time is estimated to be from 0.066 to 0.660 s, based on the mean velocity in the chamber. Therefore, the total residence time for the fluids passing the inlet chamber and microchannel is from 0.093 to 0.930 s, which is believed to be much longer than the reaction time of the solutions of sulfuric acid and sodium bicarbonate and the effect of chemical reaction kinetics is considered to be relatively insignificant. The relatively long residence time in the inlet chamber, suggests that the chemical reaction should have been completed by the time of fluid enters the microchannel. However, the mixing in the inlet chamber is far from complete; therefore, significant chemical reactions occur in the channel, especially for the diverging one.

Fig. 3(a), 3(b) and 3(c) illustrate the development of two-phase flow pattern in the converging and diverging microchannels for the reactants concentration at the inlet before mixing, C, of 0.2, 0.5 and 0.8 mol/L, respectively, for three different flow rates. In these figures, regions 1

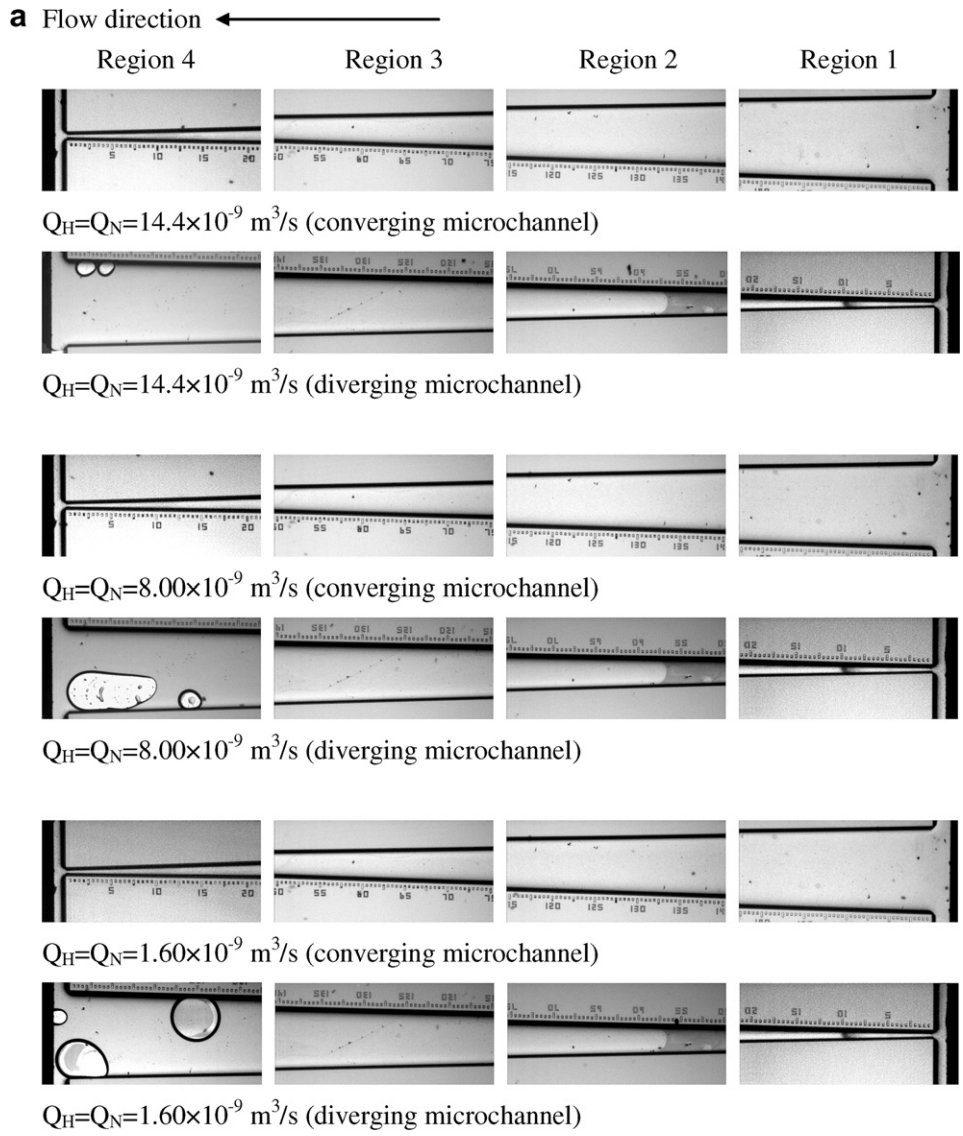

Fig. 3. Effect of flow rate on the evolution of two-phase flow pattern in both converging and diverging microchannels: (a) $C = 0.2$ mol/L, (b) $C = 0.5$ mol/L, (c) $C = 0.8$ mol/L.

and 4 are right next to the inlet or right before the outlet chamber, respectively, and regions 2 and 3 are located at about one third and two thirds of the axial distance from the channel inlet. These figures clearly demonstrate much more intensive chemical reactions in the diverging microchannel than that in the converging microchannel. For $C = 0.2$ mol/L and 1.60×10^{-9} m^3/s $\leqq Q_H = Q_N \leqq 16.0 \times 10^{-9}$ m^3/s, $C = 0.5$ mol/L, 9.60×10^{-9} m^3/s $\leqq Q_H = Q_N \leqq 16.0 \times 10^{-9}$ m^3/s, there is no bubble produced in the converging microchannel. For those cases, the concentration is too low and the flow rate is too high, considering the accelerating effect, to allow enough chemical reactions to produce a CO_2 bubble. It should also be noted that the solubility of CO_2 in the H_2O is relatively high and a small amount of CO_2 produced may dissolve in water and is not observable. At a high flow rate of $Q = 14.4 \times 10^{-9}$ m^3/s, the average liquid velocity is 0.37 m/s at the channel inlet and 3.84 m/s at the exit in the converging microchannel. Large spherical bubbles are generated in the regions near the entrance for high concentrations and low flow rates. Due to the accumulation of CO_2 produced in the upstream regions and the acceleration effect, the flow evolves to slug flow in region 3 and region 4. This is consistent with the work of Hwang et al. [12], who reported the elongation of bubble slug in an adiabatic converging microchannel with a mean hydraulic diameter of 122 μm without chemical reactions. Significantly, bubbles tend to be generated in the boundary layer near the wall, at which the reactants move slower than the bulk flow and thus have longer duration time for chemical reactions to take place. This may also be caused by the catalytic effect of the solid wall material [14].

On the other hand, bubbles are generated in the region 4 even for the lowest concentration at a relatively high flow rate in the diverging microchannel. Significantly, bubbles are formed near the wall possibly due to the reversed flow

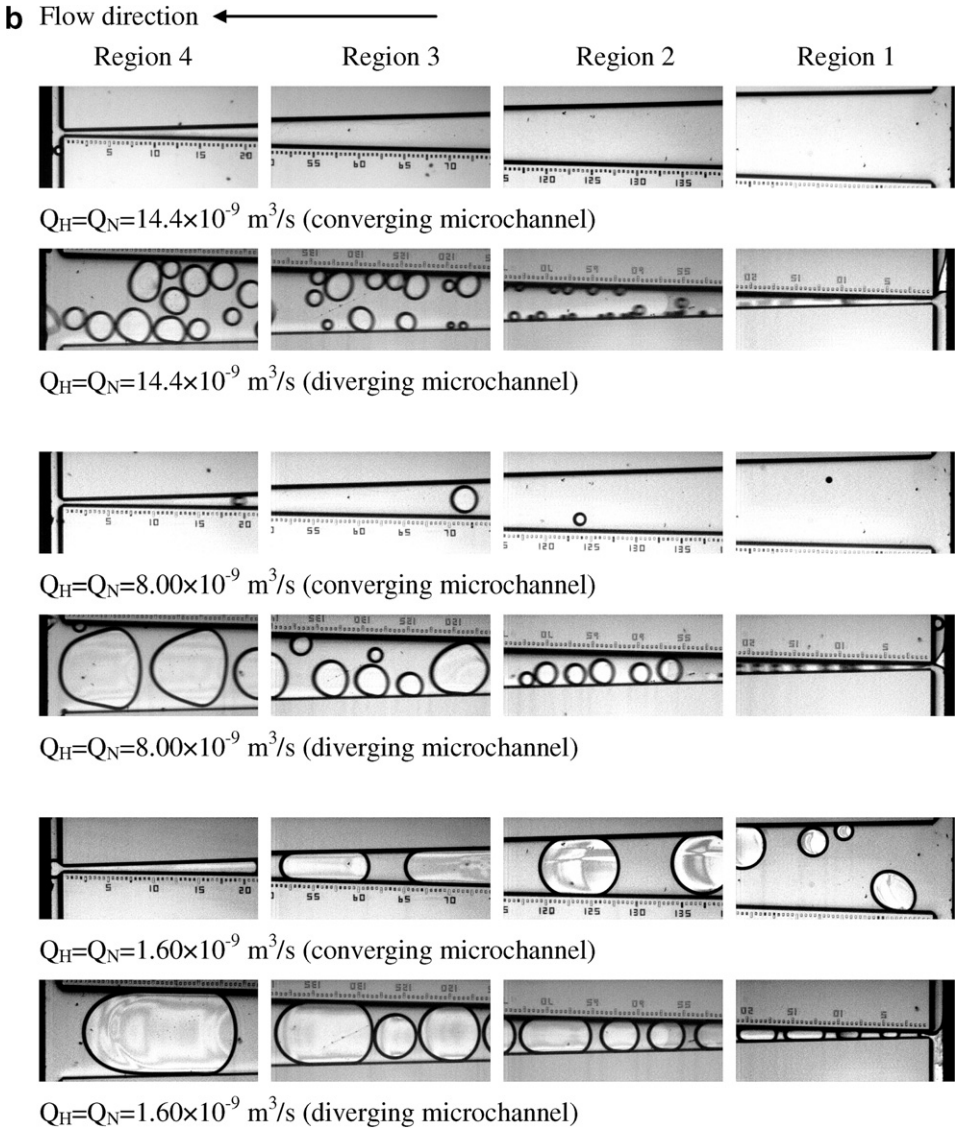

Fig. 3 (*continued*)

induced by the boundary layer separation near the exit. In general, the deceleration effect in the diverging microchannel results in much more active reactions in the regions near the exit and many bubbles, large in the center and small in the peripheral, are produced in those regions. Slug flow with large bubble slugs tends to appear in most parts of the diverging microchannel for high inlet concentrations.

The narrow entrance of the diverging microchannel may also possibly promote mixing of reactants in the inlet chamber and contribute partially to the more active reactions in the diverging microchannel. The mixing effect is supported by the generation of bubbles in the inlet chamber. Another test using $NaHCO_3$ and bromothymol blue solution also confirms the mixing effect in the inlet chamber of the diverging microchannel. The reaction of sodium bicarbonate solution (transparent) and bromothymol blue solution (brown) produces a color change to blue. Such blue fluid then flows downstream through the narrow entrance part of the diverging microchannel with little mixing. On the other hand, the same test demonstrates little mixing effect in the inlet chamber of the converging microchannel due to its large entrance area. Significant mixing effect occurs in the exit chamber of the converging microchannel. Further discussion on the mixing effect in the inlet chamber is given in the next section with the measurement of void fraction in the inlet and outlet regions, i.e., regions 1 and 4.

More detailed presentations and discussion on the development of two-phase flow pattern were given in Fu et al. [15].

It is interesting to delineate differences and similarities in two-phase flow patterns to convectional scale and other microscale configurations. Compared to the conventional channel, the two-phase flow pattern in a microchannel is characterized by the predominance of slug flow and various different kinds of annular two-phase flow [6,8]. Bubbly flow

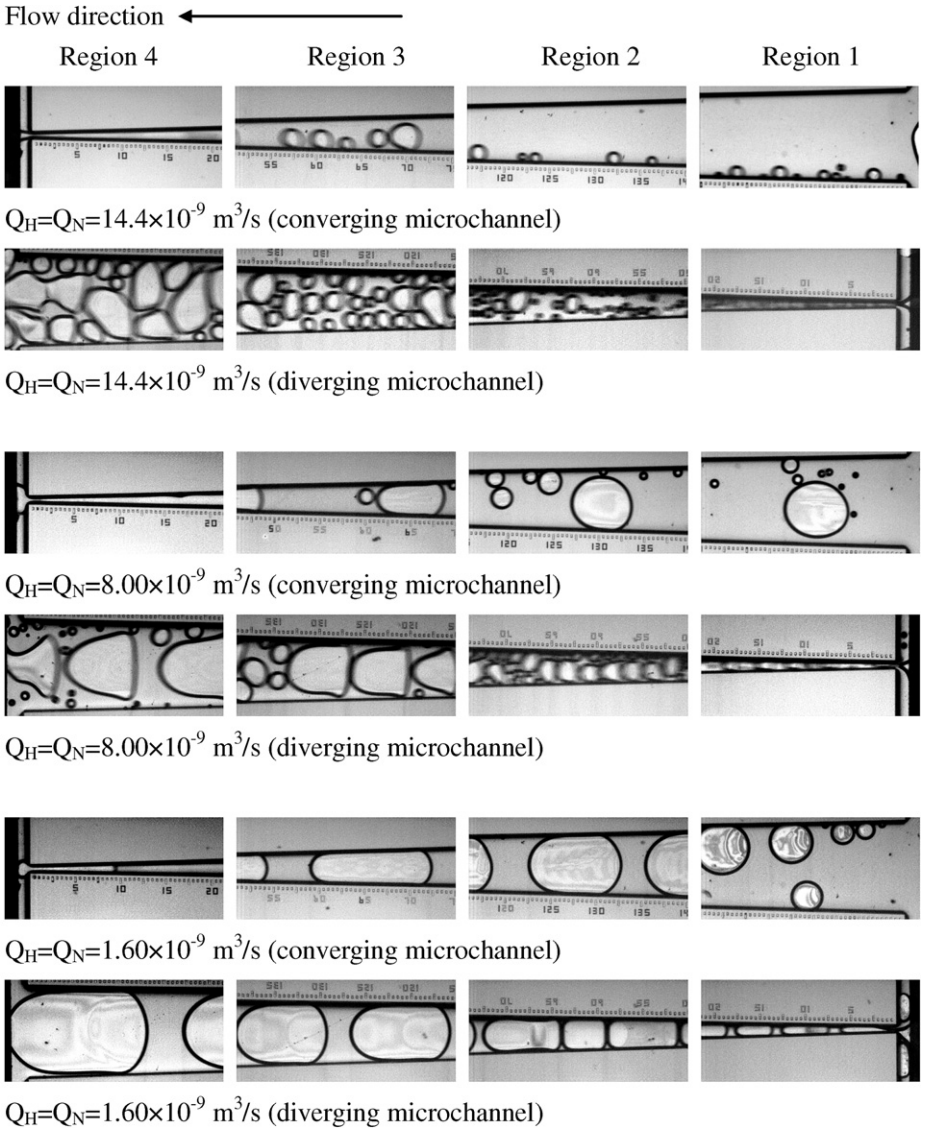

Fig. 3 (*continued*)

is rarely observed unless under very low gas flow conditions. Moreover, for slug flow, unlike that in a conventional channel, there are usually no small bubbles in the liquid slug between two neighboring elongated bubbles but strong liquid circulation may be present there [16]. There are no bubbles neither in the thin liquid film between the bubble and channel wall. Under certain circumstances, bubble train slug flow with two to three or more bubbles connecting together with the membrane between two neighboring bubbles [6].

The channel configuration may significantly affect the two-phase flow pattern in a microchannel. As stated earlier in the Introduction section, the acceleration effect in an adiabatic converging microchannel with constant gas quality may lengthen the bubbles in slug flow, while the deceleration effect in an adiabatic diverging microchannel may shorten the bubbles in slug flow. Moreover, bubble interactions due to relative motion are frequently observed in both types of microchannels [12]. As for the converging and diverging microchannels with gas bubbles produced by chemical reactions as in the present study, it can be seen that both bubbly flow and slug flow are frequently observed. The very presence of the bubbles may stir the flow and result in better mixing and producing more bubbles. Strong interactions are present in the diverging microchannel due to deceleration effect and continuous bubble productions.

3.2. Void fraction in the channel inlet and outlet regions

As stated previously, the void fraction in the channel inlet and outlet regions, i.e., region 1 and region 4, respectively, was determined by the mean value of the projected area of bubbles on the bottom wall of fifty frames randomly selected divided by the bottom surface area of the region. The length of both inlet and outlet regions under

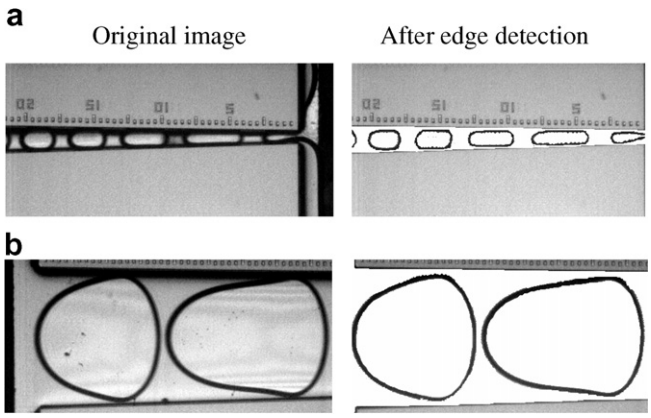

Fig. 4. Example of void fraction determination in the inlet and outlet regions in the diverging microchannel. Note that bubbles in the inlet and outlet chambers are excluded after edge detection ($C = 0.8$ mol/L, $Q_H = Q_N = 1.60 \times 10^{-9}$ m^3/s). (a) Void fraction of this image = 0.449, (b) void fraction of this image = 0.689.

consideration is about 2 mm. Figs. 4(a) and 4(b) illustrate an example of how the projected area of bubbles for both the inlet and outlet regions in the diverging microchannel was determined by Image Pro. The void fraction thus obtained for the inlet region of this particular frame is 0.449, while it is 0.689 for the outlet region for $C = 0.8$ mol/L and $Q_H = Q_N = 1.60 \times 10^{-9}$ m^3/s. It is also interesting to note that different two-phase flow pattern may result in approximately the same void fraction. Figs. 5(a) and 5(b) demonstrate significantly different flow pattern, bubbly and slug flow, respectively, resulting in approximately the same void fraction of 0.553 and 0.568, respectively.

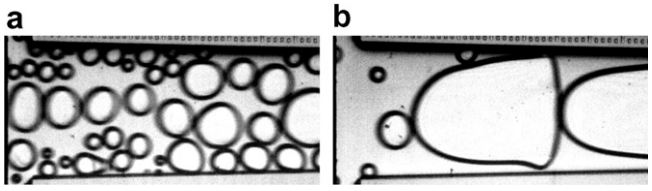

Fig. 5. Different flow pattern resulting in approximately the same void fraction: (a) bubbly flow, (b) slug flow.

Tables 1(a) and 1(b) list the void fraction for the inlet and outlet regions in the converging and diverging microchannels, respectively, as a function of inlet concentration and flow rate. For the lowest inlet concentration, i.e., $C = 0.2$ mol/L, there is no bubble generated in the inlet chamber and the void fraction in the inlet region of both converging and diverging microchannels is zero. For higher inlet concentrations, the void fraction in the inlet region results from the CO_2 generated in the inlet chamber due to chemical reactions there. Tables 1(a) and 1(b) demonstrate that the inlet void fraction for the diverging microchannel is significantly higher than that for the converging microchannel. This signifies the stronger mixing effect in the inlet chamber of the diverging microchannel due to its narrow inlet as discussed earlier in the previous section. On the other hand, the void fraction for the outlet region is a combined result of those CO_2 produced in the inlet chamber and microchannel itself. Again, in general, the outlet void fraction for the diverging microchannel is significantly higher than that for the converging one. As revealed by two-phase flow pattern, a small void fraction with significant deviation is present in the outlet region of the diverging microchannel even for the lowest concentration of $C = 0.2$ mol/L. Such a void fraction is mainly due to the flow effect in the microchannel itself as there are no bubbles generated in the inlet chamber. As discussed earlier, the deceleration effect in the diverging microchannel may result in longer duration for fluids near the exit and possible boundary layer separation. This is because the Reynolds number being relatively small (~5 at the exit) and the microchannel is relatively long compared to the mean hydraulic diameter, the adverse pressure gradient may cause boundary layer separation near the exit of the diverging microchannel with relatively small included angle [17] and results in reversed flow and significant mixing effect near the channel wall. Consequently, CO_2 bubbles may be generated in the near wall region. Interestingly, Table 1(b) indicates for the lowest inlet concentration the void fraction at the exit increases with increasing the flow rate first and reaches a maximum for $Q_H = Q_N = 6.40 \times 10^{-9}$ m^3/s. Subsequently, the mean void fraction decreases with increasing the volume flow rate. This suggests that the

Table 1(a)
Void fraction for the inlet and outlet regions in the converging microchannel

$Q_H = Q_N$ (10^{-9} m^3/s)	0.2 mol/L			0.5 mol/L			0.8 mol/L		
	α_{in}	α_{out}	$\alpha_{out} - \alpha_{in}$	α_{in}	α_{out}	$\alpha_{out} - \alpha_{in}$	α_{in}	α_{out}	$\alpha_{out} - \alpha_{in}$
1.60	0	0	0	0.040 ± 0.020	0.320 ± 0.084	0.280	0.287 ± 0.058	0.623 ± 0.116	0.336
3.20	0	0	0	0.019 ± 0.014	0.188 ± 0.075	0.169	0.070 ± 0.032	0.570 ± 0.107	0.500
4.80	0	0	0	0.005 ± 0.007	0.097 ± 0.053	0.092	0.049 ± 0.027	0.433 ± 0.107	0.384
6.40	0	0	0	0.001 ± 0.002	0.029 ± 0.039	0.028	0.048 ± 0.030	0.394 ± 0.126	0.346
8.00	0	0	0	0	0.012 ± 0.013	0.012	0.046 ± 0.026	0.224 ± 0.094	0.178
9.60	0	0	0	0	0	0	0.025 ± 0.022	0.209 ± 0.090	0.184
11.2	0	0	0	0	0	0	0.024 ± 0.027	0.181 ± 0.087	0.157
12.8	0	0	0	0	0	0	0.005 ± 0.003	0.173 ± 0.093	0.168
14.4	0	0	0	0	0	0	0.008 ± 0.003	0.153 ± 0.087	0.145
16.0	0	0	0	0	0	0	0.005 ± 0.002	0.139 ± 0.076	0.134

Table 1(b)
Void fraction for the inlet and outlet regions in the diverging microchannel

$Q_H = Q_N$ (10^{-9} m^3/s)	0.2 mol/L			0.5 mol/L			0.8 mol/L		
	α_{in}	α_{out}	$\alpha_{out} - \alpha_{in}$	α_{in}	α_{out}	$\alpha_{out} - \alpha_{in}$	α_{in}	α_{out}	$\alpha_{out} - \alpha_{in}$
1.60	0	0.023 ± 0.013	0.023	0.287 ± 0.081	0.486 ± 0.056	0.199	0.364 ± 0.107	0.664 ± 0.034	0.300
3.20	0	0.079 ± 0.020	0.079	0.141 ± 0.077	0.484 ± 0.027	0.343	0.240 ± 0.096	0.621 ± 0.035	0.381
4.80	0	0.128 ± 0.008	0.128	0.126 ± 0.038	0.464 ± 0.041	0.338	0.228 ± 0.085	0.536 ± 0.041	0.308
6.40	0	0.149 ± 0.013	0.149	0.129 ± 0.012	0.449 ± 0.028	0.320	0.141 ± 0.051	0.540 ± 0.038	0.400
8.00	0	0.146 ± 0.011	0.146	0.088 ± 0.020	0.420 ± 0.024	0.332	0.125 ± 0.050	0.541 ± 0.034	0.416
9.60	0	0.052 ± 0.012	0.052	0.078 ± 0.007	0.334 ± 0.037	0.256	0.087 ± 0.042	0.549 ± 0.046	0.462
11.2	0	0.086 ± 0.005	0.086	0.061 ± 0.018	0.181 ± 0.021	0.120	0.077 ± 0.034	0.524 ± 0.044	0.447
12.8	0	0.054 ± 0.005	0.054	0.044 ± 0.011	0.242 ± 0.046	0.198	0.065 ± 0.028	0.521 ± 0.050	0.456
14.4	0	0.013 ± 0.005	0.013	0.042 ± 0.010	0.123 ± 0.039	0.081	0.054 ± 0.021	0.491 ± 0.041	0.437
16.0	0	0.014 ± 0.003	0.014	0.019 ± 0.013	0.187 ± 0.025	0.168	0.052 ± 0.024	0.398 ± 0.060	0.346

boundary layer separation effect is dominated for low flow rates, while the short fluid duration effect at high flow rates overcome that due to the boundary layer separation. Should the inlet concentration is higher; the void generation in the outlet region due to the diverging effect will be much more significant.

Tables 1(a) and 1(b) also present the difference in void fraction between outlet and inlet regions, which reflects the CO_2 generated in the channel. The tables clearly demonstrate that the void fraction difference for the diverging microchannel is generally much higher than that for the converging one especially for those cases with high flow rates. The bubbles produced in the inlet chamber may result in jet-like gas flow in the microchannel and cause significant agitation effect and, therefore, active chemical reactions in the channel. To examine such an effect of gas flow at the channel inlet on the evolution of void fraction in the channel, Fig. 6 illustrates the void fraction difference between the outlet region and inlet region versus the void fraction at the inlet region for both types of microchannel. The figure clearly indicates that the void fraction increment in the channel increases rapidly with increase in the void fraction in the inlet region (α_{in}) and reaches a maximum of about 0.5 for $\alpha_{in} = 0.09$. For $\alpha_{in} > 0.09$, the void fraction increment in the channel decreases with increase in α_{in}.

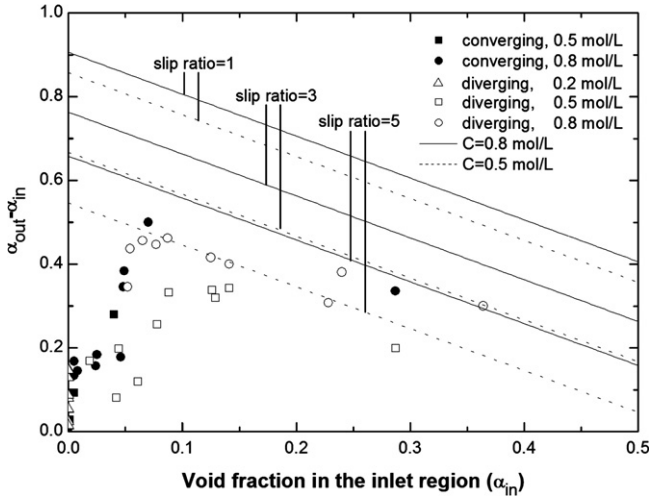

Fig. 6. The void fraction difference between the outlet region and inlet region versus the void fraction in the inlet region for both types of microchannel.

The rapid increase of void fraction increment for low void fractions in the inlet region suggests the significant bubble agitation effects and thus the CO_2 generated in the microchannel, no matter whether the microchannel is converging or diverging. However, it should be noted that for the outlet region of the converging microchannel and the inlet region of the diverging one, the channel is very narrow and a small amount of gas quality may fill the channel and result in a relatively large void fraction. The decrease of void fraction increment in the channel for $\alpha_{in} > 0.09$ suggests that the void fraction in the outlet region may approach its asymptotic limit. Indeed, Fig. 6 also shows the void fraction increments if the sodium bicarbonate is totally consumed at the channel exit for the slip ratio between gas and liquid flow of 1, 3 and 5, respectively. As stated earlier, in the section of Experimental Procedure, the volume flow rate of CO_2 thus produced would be from 7.69×10^{-9} to 308×10^{-9} m^3/s, depending on the flow rate and inlet concentration. The void fraction of CO_2 bubbles can be evaluated given the gas flow rate and slip ratio. Fig. 6 shows that a slip ratio of 3–5 may predict fairly the void increment versus the void fraction in the inlet region for $\alpha_{in} > 0.09$. For the present atmospheric pressure systems, a slip ratio of 3 to 5 seems to be quite reasonable. However, it should also be noted that incomplete mixing could also limit the production and, therefore, the void fraction of CO_2 in the microchannel.

3.3. Single-phase flow pressure drop

As indicated earlier, no bubbles are generated for low inlet concentrations in the converging microchannel and single phase flow of solution mixture prevails. As for the diverging microchannel, only a small amount of bubbles are generated intermittently in the outlet region. Therefore, it may be approximated as single-phase flow; as such a small amount of bubbles is considered to have insignificant effect on the frictional pressure drop. Figs. 7(a) and 7(b) illustrate the single-phase flow pressure drop, for

$C = 0.2$ mol/L, for the converging and diverging microchannels, respectively, which includes the inlet and outlet losses due to sudden contraction and sudden expansion, respectively, acceleration pressure drop and frictional one:

$$\Delta P_{\text{total}} = \Delta P_{\text{f}} + \frac{1}{2}\rho(V_{\text{out}}^2 - V_{\text{in}}^2) + \Delta P_{\text{in}} + \Delta P_{\text{out}} \tag{2}$$

where ΔP_{in} and ΔP_{out} represent the pressure loss at the inlet and outlet due to sudden contraction and expansion, respectively, and may be evaluated by appropriate equations [12].

Fig. 7(a) indicates that the inlet pressure loss due to sudden contraction is minor and negligible; the exit pressure loss and acceleration pressure loss are approximately the same and are in the order of 10 kPa for the converging microchannel. On the other hand, Fig. 7(b) indicates that for the diverging one, the inlet and outlet pressure losses due to sudden contraction and expansion, respectively, are minor and negligible; the acceleration pressure loss is in the order of −10 kPa. The frictional pressure drop for both types of microchannel, which may be obtained by deducting inlet/outlet losses and acceleration pressure drop from the total pressure drop, is most dominant as one may expect.

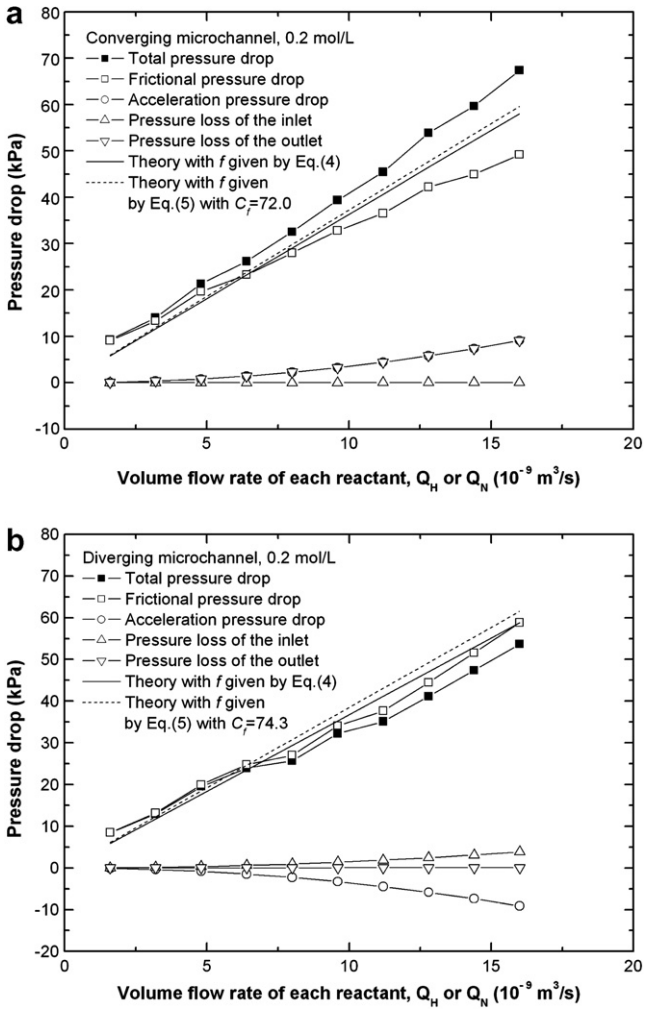

Fig. 7. Single-phase pressure drop of the (a) converging, and (b) diverging microchannel for $C = 0.2$ mol/L.

Since the converging or diverging angle of the microchannel is relatively small for the present work, the Reynolds number corresponding to the range of flow rate ranges from 13.1 to 131 at $C = 0.2$ mol/L. The flow in the microchannel may be assumed laminar and the frictional pressure drop may be approximately evaluated by the following equation:

$$\Delta P_{\text{f}} = \int_0^L \left(\frac{1}{2}\rho V(z)^2 f(z)\frac{1}{D_{\text{H}}(z)}\right) \mathrm{d}z \tag{3}$$

Assume the Hagen–Poiseuille equation is applicable for the rectangular channel used in the present study; the frictional factor may be evaluated by the following equation [18]:

$$f = \frac{96(1 - 1.3553\gamma + 1.9467\gamma^2 - 1.7012\gamma^3 + 0.9564\gamma^4 - 0.2537\gamma^5)}{Re} \tag{4}$$

where γ is the aspect ratio of the depth to the width of the channel, which is axial-location dependent for the microchannel of this study. Hwang et al. [12] reported that the frictional pressure drop may be fitted with the frictional factor simply evaluated by the following equation:

$$f = \frac{C_{\text{f}}}{Re} \tag{5}$$

where C_{f} is a fitting constant. The Reynolds number in above equations is evaluated based on mean diameter and mean velocity and the mixture density (ρ_{L}) and viscosity (μ_{L}) of the solution of sulfuric acid and sodium bicarbonate [10,19].

Fig. 7 indicates that Eq. (5) with $C_{\text{f}} = 72.0$ and 74.3, respectively, may predict the single-phase frictional pressure drop within 20% and 15%, respectively, for the converging and diverging microchannels and there is good agreement between predictions from Eqs. (4) and (5).

3.4. Two-phase flow pressure drop

Fig. 8(a) displays the total pressure drop in the converging microchannel as a function of inlet concentration and volume flow rate. The figure clearly shows that the pressure drop increases approximately linearly with increase in flow rate and the presence of CO_2 bubbles in the channel does not increase the pressure drop significantly. As discussed earlier, the chemical reactions in the converging microchannel is relatively mild and only a small amount of CO_2 bubbles are produced in the channel. Moreover, the bubbles generated at high inlet concentration are quite large and the interfacial area density is expected to below. Consequently, the increase in the pressure drop due to the inlet concentration is quite insignificant in the converging microchannel.

The effect of inlet concentration on the pressure drop is much more significant in the diverging microchannel.

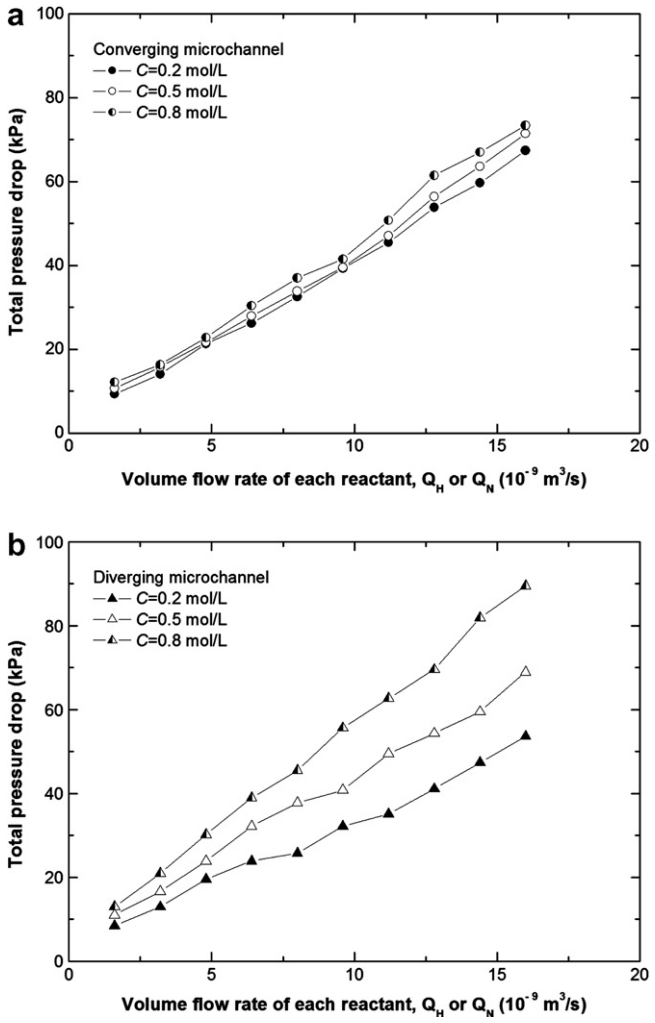

Fig. 8. Total pressure drop in the (a) converging, and (b) diverging microchannel.

Fig. 8(b) exhibits the pressure drop in the diverging microchannel as a function of inlet concentration and flow rate. As for the converging microchannel, the pressure drop increases approximately linearly with increase in flow rate. However, the effect of the inlet concentration on the pressure drop is much more significant than that for the converging microchannel. As presented and discussed previously, the deceleration and the possible boundary separation effect in the diverging microchannel tends to promote chemical reactions and much more CO_2 bubbles are produced in the channel. Consequently, the increase in pressure drop owing to the inlet concentration is much more significant than that for the converging microchannel. For $Q = 14.4 \times 10^{-9}$ m^3/s, the total pressure drop for $C = 0.8$ mol/L is 81.9 kPa, that is about 1.72 times of that for $C = 0.2$ mol/L and the same flow rate. At this flow rate, for $C = 0.8$ mol/L, as shown earlier in Fig. 3(c), many bubbles are generated in the diverging microchannel, while, for $C = 0.2$ mol/L, the flow is basically single phase. It is evident that the pressure drop multiplication due to CO_2 bubble appears to be mild, though significant.

Indeed, comparing Fig. 8(a) with Fig. 8(b) reveals that the increase of pressure drop due to significant bubble generation in the diverging microchannel is counter-balanced by the deceleration effect. In fact, for $C = 0.2$ and 0.5 mol/L at a given flow rate, the pressure drop through the diverging microchannel is smaller than that in the converging microchannel, where there are no bubbles or very few bubbles. This shows a merit of the diverging microchannel design for the removal of CO_2 bubbles in a microchannel.

Using the void fraction measured for the inlet and outlet regions and the quality evaluated assuming homogeneous two-phase flow, i.e., with unity slip ratio, the acceleration pressure drop and pressure losses at the inlet and outlet may be evaluated, see the equations in Hwang et al. [12]. As a result, the frictional pressure drop through the channel may be determined by subtracting the acceleration pressure drop and inlet/outlet pressure losses from the total pressure drop. Figs. 9(a) and 9(b) display the various components of pressure drop as a function of the volume flow

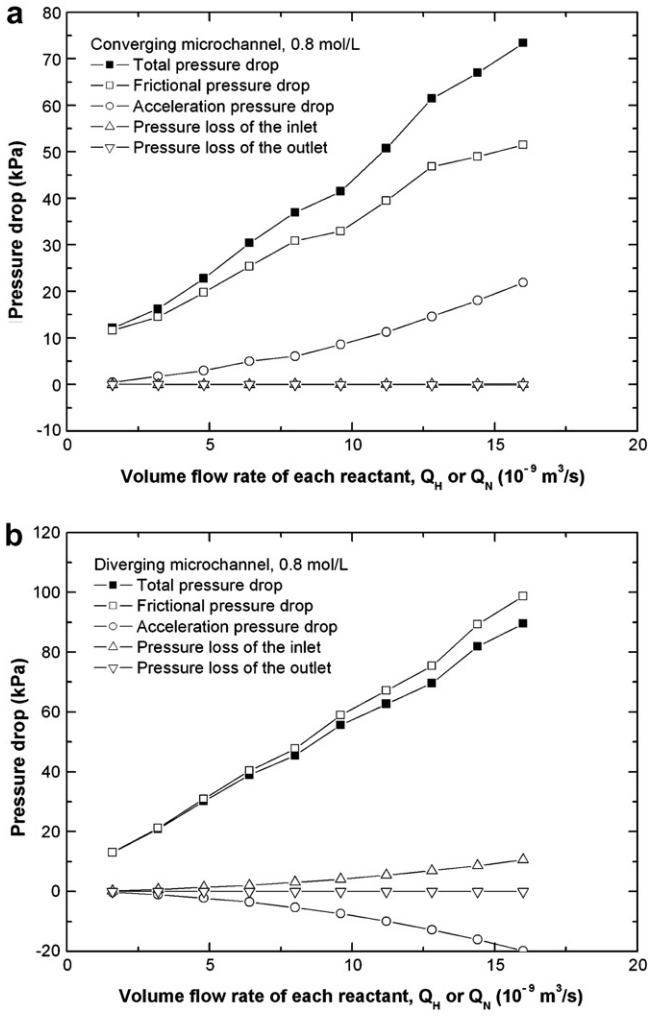

Fig. 9. The various components of pressure drop as a function of volume flow rate for the (a) converging, and (b) diverging microchannel for $C = 0.8$ mol/L.

rate for the converging and diverging microchannels, respectively for $C = 0.8$ mol/L. The figures demonstrate that frictional pressure drop is most dominant; the acceleration pressure drop contributes almost one quarter of the total pressure drop positively and negatively for the converging and diverging microchannels, respectively; and the inlet and outlet pressure losses due to sudden area change is negligible. Note that for the diverging microchannel the frictional pressure drop is higher than the total pressure drop due to deceleration effect in the channel.

It is interesting to present the data of two-phase frictional pressure drop in terms of two-phase frictional multiplier defined as

$$\phi_{\mathrm{L}}^2 = \frac{\Delta P_{\mathrm{f},2\phi}}{\Delta P_{\mathrm{f,L}}} \tag{6}$$

where $\Delta P_{\mathrm{f,L}}$ is the frictional pressure drop for the liquid flowing alone through the same channel. It is understood that void fraction and so the local frictional multiplier in the microchannel is changing due to CO_2 generation and pressure variation. The two-phase frictional multiplier defined in above equation can be considered as the mean value. For the converging microchannel, single-phase liquid flow prevails for the case of the $C = 0.2$ mol/L the pressure drop for $C = 0.2$ mol/L is, therefore, chosen as the reference for $C = 0.5$ and 0.8 mol/L, respectively, with mixture viscosity evaluated based on the equation given in [10,19]. For the diverging microchannel, the frictional pressure drop for the case of $C = 0.2$ mol/L is also selected as the reference, though small CO_2 bubbles may be produced intermittently in the outlet region. Fig. 10 illustrates the two-phase frictional multiplier as a function of the mean void fraction in the channel, i.e., the average of void fraction in the inlet and outlet regions. For the converging microchannel, the multiplier is from 0.95 to 1.10 indicating that for some cases the two-phase frictional pressure drop may be slightly smaller than the single-phase flow frictional pressure drop. This may be owing to the over-prediction of acceleration pressure drop assuming homogeneous two-phase flow. For the diverging microchannel, the two-phase multiplier is from 1.2 to 1.6. For both types of microchannel, the two-phase frictional multiplier may be positively correlated with the mean void fraction in the channel linearly within ±15% as show in the Fig. 10.

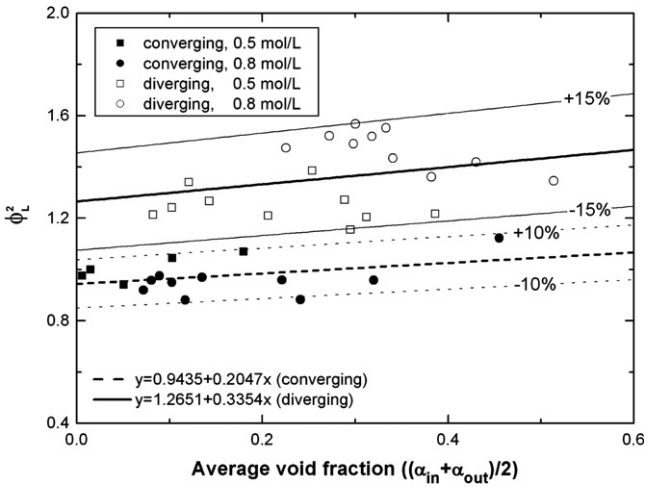

Fig. 10. The two-phase frictional multiplier as a function of the average void fraction in the channel.

The two-phase frictional multiplier is usually correlated as a function of quality or the Lockhart–Martinelli parameter. However, in the present study, only the void fractions at the channel inlet and outlet regions were measured. By assuming homogeneous two-phase flow, i.e., a unity slip ratio, the quality of CO_2 may be evaluated by the following fundamental equation:

$$x = \left[1 + \frac{\rho_{\mathrm{L}}}{\rho_{\mathrm{G}}}\frac{(1-\alpha)}{\alpha}\right]^{-1} \tag{7}$$

where ρ_{L} is the density of the liquid mixture and ρ_G is the density of CO_2 in the region. The mean quality of CO_2 flow in the microchannel may be approximated by the average of qualities at inlet and outlet regions:

$$x_{\mathrm{ave}} = \frac{x_{\mathrm{in}} + x_{\mathrm{out}}}{2} \tag{8}$$

For the present study, the average quality of CO_2 in the converging and diverging microchannel range from 1.07×10^{-5} to 1.82×10^{-3} and 1.85×10^{-4} to 2.26×10^{-3}, respectively. Since the flow rate in the present study is relatively small, the flow for each phase alone will be laminar. The Lockhart–Martinelli parameter (X) may be expressed as

$$X^2 = \left(\frac{\rho_{\mathrm{G}}}{\rho_{\mathrm{L}}}\right)\left(\frac{\mu_{\mathrm{L}}}{\mu_{\mathrm{G}}}\right)\frac{(1-x_{\mathrm{ave}})}{x_{\mathrm{ave}}} \tag{9}$$

Fig. 11 illustrates that the correlation of Hwang et al. [12] compares fairly well with the both sets of data for the converging and diverging channel, respectively. It is interesting to note that the correlations of Hwang et al. were developed for adiabatic two-phase flow in converging and diverging microchannels:

$$\phi_{\mathrm{L}}^2 = 1 - \frac{2.64}{X} + \frac{47.53}{X^2} \quad \text{(converging microchannel)} \tag{10}$$

$$\phi_{\mathrm{L}}^2 = 1 + \frac{9.01}{X} + \frac{1}{X^2} \quad \text{(diverging microchannel)} \tag{11}$$

The data of the converging microchannel may also be predicted well by the correlation of Mishima and Hibiki [3]:

$$\phi_{\mathrm{L}}^2 = 1 + \frac{M}{X} + \frac{1}{X^2} \tag{12}$$

$$M = 21(1 - \mathrm{e}^{-0.319 D_{\mathrm{H}}}) \tag{13}$$

On the other hand the data of the diverging microchannel compares very well with the Chisholm's equation with the constant (M) of 5 [20], which is typical for the case of each phase flow above being laminar:

$$\phi_{\mathrm{L}}^2 = 1 + \frac{M}{X} + \frac{1}{X^2} \tag{14}$$

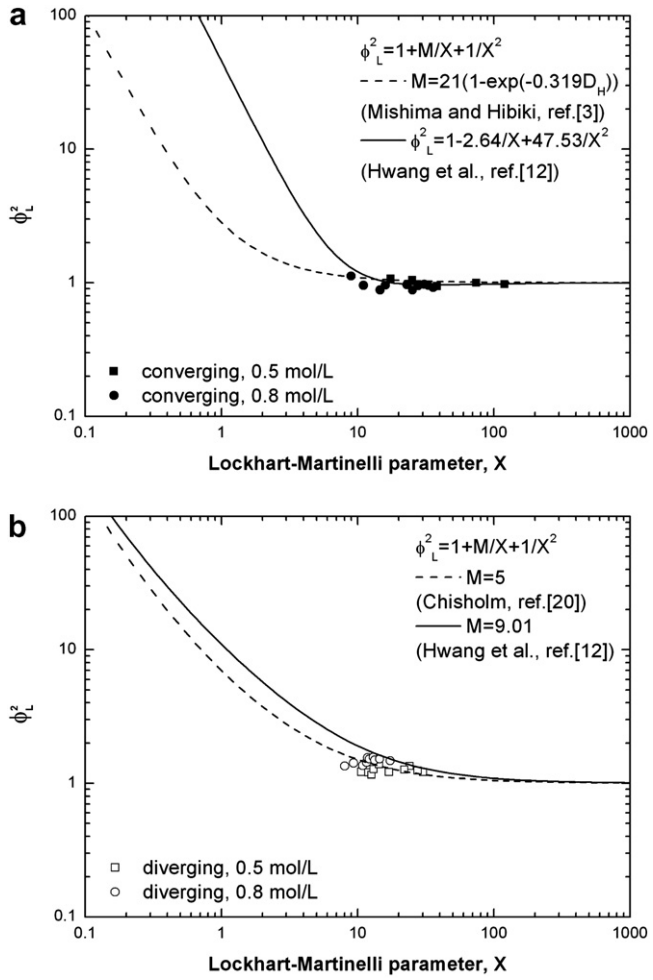

Fig. 11. Variation of two-phase frictional multiplier data with Lockhart–Martinelli parameter: (a) converging, (b) diverging microchannel.

4. Summary and conclusions

The present study investigates experimentally the evolution of two-phase flow pattern, void fraction in the inlet and outlet regions, and pressure drop in the converging and diverging silicon-based microchannels with CO_2 bubbles produced by the chemical reactions of sulfuric acid and sodium bicarbonate. The effects of the reactants' concentrations and the flow rates of the solutions are studied. The following conclusions may be drawn from the results of the present work:

1. Flow visualization demonstrates that the present design of microchannel, with the inlet chamber, results in much more intensive chemical reactions in the diverging microchannel than that in the converging one.
2. The appearance of CO_2 bubbles, without bubble generation in the inlet chamber, near the exit of the diverging microchannel for the lowest inlet concentration of $C = 0.2$ mol/L of this study, in contrast to no bubble generation in the converging one, indicates that, irrespective of the design of inlet geometry, the deceleration effect in the diverging microchannel may intensify chemical reactions possibly due to better mixing effect and flow reversal caused by boundary layer separation. The latter effect is also evident as many small bubbles are generated near the channel wall for high inlet concentrations and /or low flow rates in the diverging microchannel.
3. The present design of the inlet chamber may result in significant mixing effect and generation of CO_2 bubbles in the inlet chamber itself, especially for the diverging microchannel with narrow inlet.
4. The measurement and analysis of the void fraction in the inlet and outlet regions indicate that the presence of small void fraction, <0.1, at the inlet may promote CO_2 generation in the microchannel, irrespective of the channel is converging or diverging. This suggests the agitation effects of bubble flow in the microchannel.
5. For low inlet concentrations there are no or little bubbles generated and the corresponding single-phase flow frictional pressure drop may be well predicted by the Hagen-Poiseuille equation with frictional factor depending on the aspect ratio.
6. The increase of inlet concentration of reactants does not increase the pressure drop significantly in the converging microchannel as the CO_2 generation is significantly suppressed.
7. The inlet concentration presents significant effects on the pressure drop in the diverging microchannel as CO_2 bubbles generation is greatly intensified.
8. The increase of pressure drop due to significant bubble generation in the diverging microchannel is counter-balanced by the deceleration effect; therefore, the pressure drop multiplication due to CO_2 bubbles is quite mild. This shows a merit of a diverging microchannel design for the removal of CO_2 bubbles in a microchannel.
9. The two-phase frictional multiplier may be positively correlated with the mean void fraction in the channel linearly, and the data agree well with predictions from the correlations in the literature.

Acknowledgement

This work was supported by the National Science Council of Taiwan, ROC, under the contract No. NSC 92-2212-E-007-093.

References

[1] P. Argyropulos, K. Scott, W.M. Taama, Gas evolution and power performance in direct methanol fuel cells, J. Appl. Electrochem. 29 (1999) 661–669.
[2] T. Fukano, A. Kariyasaki, Characteristics of gas–liquid two-phase flow in capillary tube, Nucl. Eng. Des. 141 (1993) 59–68.
[3] K. Mishima, T. Hibiki, Some characteristics of air–water two–phase flow in small diameter vertical tubes, Int. J. Multiphase Flow 22 (1996) 703–712.
[4] K.A. Triplett, S.M. Ghiaasiaan, S.I. Abdel-Khalik, D.L. Sadowski, Gas–liquid two-phase flow in microchannels, Part I: two-phase flow patterns, Int. J. Multiphase Flow 25 (1999) 377–394.

[5] K.A. Triplett, S.M. Ghiaasiaan, S.I. Abdel-Khalik, A. LeMouel, B.N. McCord, Gas–liquid two-phase flow in microchannels, Part II: void fraction and pressure drop, Int. J. Multiphase Flow 25 (1999) 395–410.
[6] W.L. Chen, M.C. Twu, C. Pan, Gas–liquid two-phase flow in micro-channels, Int. J. Multiphase Flow 28 (2002) 1235–1247.
[7] R.S. Stanley, R.F. Barron, T.A. Ameel, Two-phase flow in micro channels, DSC-vol. 62/354, Microelectromechanical Systems, ASME, 1997.
[8] Serizawa, Z. Feng, Z. Kawara, Two-phase flow in microchannel, Exp. Therm. Fluid Sci. 26 (2002) 703–714.
[9] P.M.-Y. Chung, M. Kawaji, The effect of channel diameter on adiabatic two-phase flow characteristics in microchannels, Int. J. Multiphase Flow 30 (2004) 735–761.
[10] B.R. Fu, C. Pan, Flow pattern transition instability in a microchannel with CO_2 bubbles produced by chemical reactions, Int. J. Heat Mass Transfer 48 (2005) 4397–4409.
[11] L. Lin, K.S. Udell, A.P. Pisano, Liquid–vapor phase transition and bubble formation in micro structure, Therm. Sci. Eng. 2 (1994) 52–59.
[12] J.J. Hwang, F.G. Tseng, C. Pan, Ethanol-CO_2 two-phase flow in diverging and converging microchannels, Int. J. Multiphase Flow 31 (2005) 548–570.
[13] D.S. Meng, J. Kim, C.J. Kim, A distributed gas breather for micro direct methanol fuel cells (μ-DMFC), in: Proceedings of the IEEE International Conference on Micro Electro Mechanical Systems (MEMS'03), Kyoto, Japan, January 19–23, 2003, pp. 534–537.
[14] C.T. Yeh, Private Communication, Department of Chemistry, National Tsing Hua University, Hsinchu, Taiwan, 2005.
[15] B.R. Fu, F.G. Tseng, C. Pan, Two-phase flow patterns in converging or diverging microchannels with CO_2 bubbles produced by chemical reactions, in: Proceedings of the Third International Conference on Microchannels and Minichannels, Toronto, Ontario, Canada, June 13–15, 2005.
[16] T.C. Thulasidas, M.A. Abraham, R.L. Cerro, Bubble-train flow in capillaries of circular and square cross section, Chem. Eng. Sci. 50 (1995) 183–199.
[17] H. Schlichting, Boundary Layer Theory, Seventh ed., McGraw-Hill Book Company, New York, 1979 (Chapter 5).
[18] J.P. Hartnett, M. Kostic, Heat transfer to Newtonian and non-Newtonian fluids in rectangular ducts, Adv. Heat Transfer 19 (1989) 247–356.
[19] J. Kendall, K.P. Monroe, The viscosity of liquids. II. The viscosity-composition curve for ideal liquid mixtures, J. Am. Chem. Soc. 39 (1917) 1787–1802.
[20] D. Chisholm, A theoretical basis for the Lockhart–Martinelli correlation for two-phase flow, Int. J. Heat Mass Transfer 10 (1967) 1767–1778.